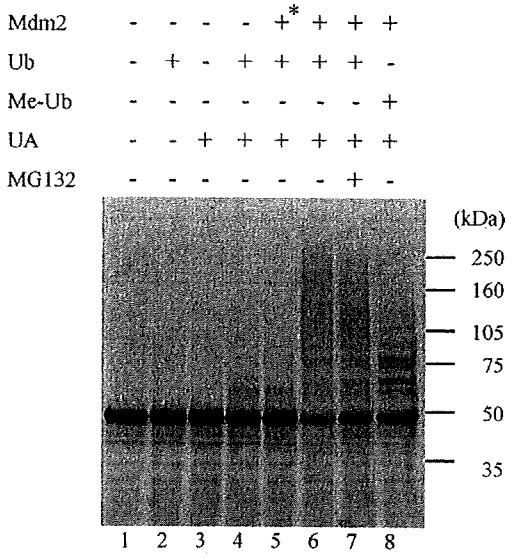

Fig. 4. *In vitro* ubiquitination of p53 using the insect cell-free protein synthesis system. Six microliters of *in vitro* translated and fluorescently labeled p53 was mixed with 4 μL of Mdm2 translated in the presence of the caspase-3 inhibitor (Ac-DEVD-CHO). *In vitro* ubiquitination assays were performed by adding Ub/Me-Ub and UA as described in Section 2. After the incubation, the total volume of the mixture was electrophoresed on a 5–20% SDS-PAGE gel. Asterisk indicates *in vitro* translated Mdm2 in the absence of the caspase-3 inhibitor.

reported to be a protein with molecular weight of about 100 kDa (Pochampally et al., 1998). This result suggested that the Mdm2 gene product was cleaved by a protease(s) in the insect cell-free protein synthesis system. To investigate this possibility further, N-terminal and C-terminal GST-tagged Mdm2 plasmids were constructed. Expression analyses of these constructs suggested that the cleavage site of the synthesized Mdm2 was located in the C-terminal region of the full-length Mdm2 protein (data not shown). The N-terminal amino acid sequence of the affinity-purified, C-terminal GST-tagged Mdm2 was NH_2-^{362}XKKTIVNPSR^{371} (data not shown). Therefore, a mutant Mdm2 construct was generated with an Ala substitution of Asp 361, and this protein escaped proteolytic degradation by an Mdm2-cleaving enzyme (data not shown). These results indicate the cleavage site of the cell-free synthesized Mdm2 is between Asp 361 and Cys 362. It has been reported that Mdm2 is cleaved by caspase-3 at the C-terminal side of the Asp 361 residue (Chen et al., 1997). Therefore, the effect of adding a caspase inhibitor on the translation product of Mdm2 was evaluated. The Mdm2-cleaving enzyme activity was almost completely inhibited by addition of the caspase-3 inhibitor (Ac-DEVD-CHO) (Fig. 5), suggesting that a caspase-like activity exists in the insect cell-free protein synthesis system.

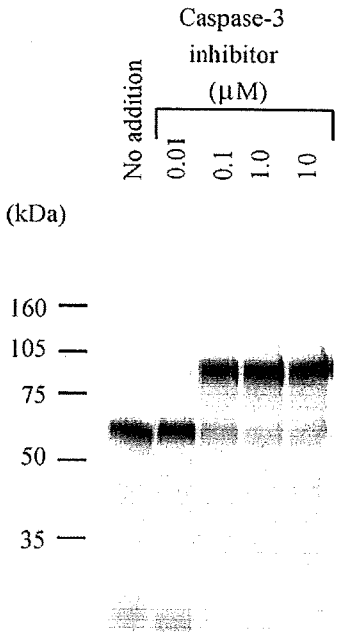

Fig. 5. A caspase-like activity in the insect cell-free protein synthesis system and its inhibition by a caspase-3 inhibitor. Fluorescent labeling of *in vitro* translated Mdm2 protein was carried out using FluoroTect as described in Section 2. Translation was performed in the presence or absence of a caspase-3 inhibitor I (Ac-DEVD-CHO). After the translation, 6 μL of the reaction mixture was electrophoresed on a 10% SDS-PAGE gel.

It has been reported that cleavage after Asp 361 by an Mdm2-specific caspase divides Mdm2 into an N-terminal fragment that binds p53 and a C-terminal RING-finger domain, resulting in loss of its E3 activity (Pochampally et al., 1999). Therefore it is likely that the inefficient Ub conjugation to p53 in the insect cell-free protein synthesis system was also owing to loss of the E3 activity of Mdm2 in this *in vitro* system. *In vitro* ubiquitination of p53 was next attempted in the insect cell-free protein synthesis system in the presence of the caspase-3 inhibitor Ac-DEVD-CHO, resulting in a remarkable acceleration of Ub conjugation to p53, presumably due to the concomitant production of full-length Mdm2 (Fig. 4: lane 6).

Mdm2-mediated ubiquitination drives p53 to proteasomal degradation (Rodriguez et al., 2000). To investigate whether the insect cell-free protein synthesis system has proteasomal activity, a proteasome inhibitor, MG132, was added to the *in vitro* ubiquitination reaction mixture. However, the addition of MG132 to the insect cell-free protein synthesis system produced only a slight effect (Fig. 4: lane 7). The addition of lactacystin, a specific proteasome inhibitor, also showed no effect on the mobility pattern of p53 on SDS-PAGE (data not shown). Further studies are necessary to clarify this finding.

It has been reported that Mdm2 mediates multiple monoubiquitinations of p53 (Lai et al., 2001). Therefore the ubiquitination reaction was performed using Me-Ub to investigate whether the type of ubiquitination generated in the insect cell-free protein synthesis system is mono- or poly-ubiquitination. Ladder bands at around 60–100 kDa were remarkably enhanced in the ubiquitination assay using Me-Ub (Fig. 4: lane 8). This result suggested that poly-ubiquitination of p53 occurred when Ub, UA, and full-length Mdm2 were added to the *in vitro* ubiquitination reaction carried out by the insect cell-free protein synthesis system.

3.3. Affinity purification of in vitro ubiquitinated p53

To evaluate the performance of insect cell-free protein synthesis system as a tool for production of Ub-conjugated proteins, *in vitro* ubiquitination of p53 was carried out using Me-Ub at a 2.5 mL reaction scale. The *in vitro* synthesized and ubiquitinated p53 was collected by affinity purification, and CBB-detectable ubiquitinated p53 proteins were thus obtained (Fig. 6). This result suggests that the insect cell-free protein synthesis system is an effective tool to prepare ubiquitinated proteins of interest.

3.4. Mass spectrometric analyses of in vitro ubiquitinated p53

The 50 kDa and ladder bands were excised individually and digested with trypsin, and these tryptic digests were analyzed by MALDI-TOF MS. Peaks detected in the mass spectrum of the tryptic digests of the 50 kDa band agreed well with the theoretical *m/z* values for the p53 protein (about 67% sequence coverage, Fig. 7A-b). The MALDI-mass spectra produced from each of the ladder

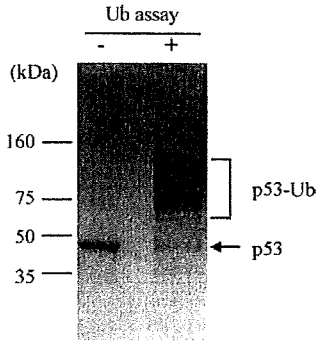

Fig. 6. SDS-PAGE of the affinity-purified p53 proteins. An *in vitro* ubiquitination reaction was carried out using Me-Ub at a 2.5 mL reaction scale. Ubiquitinated p53 was collected by affinity purification and concentrated to about 20 μL by ultrafiltration (molecular cutoff = 10 kDa). Eight microliters of the concentrate was electrophoresed on 10% SDS-PAGE and visualized by CBB staining.

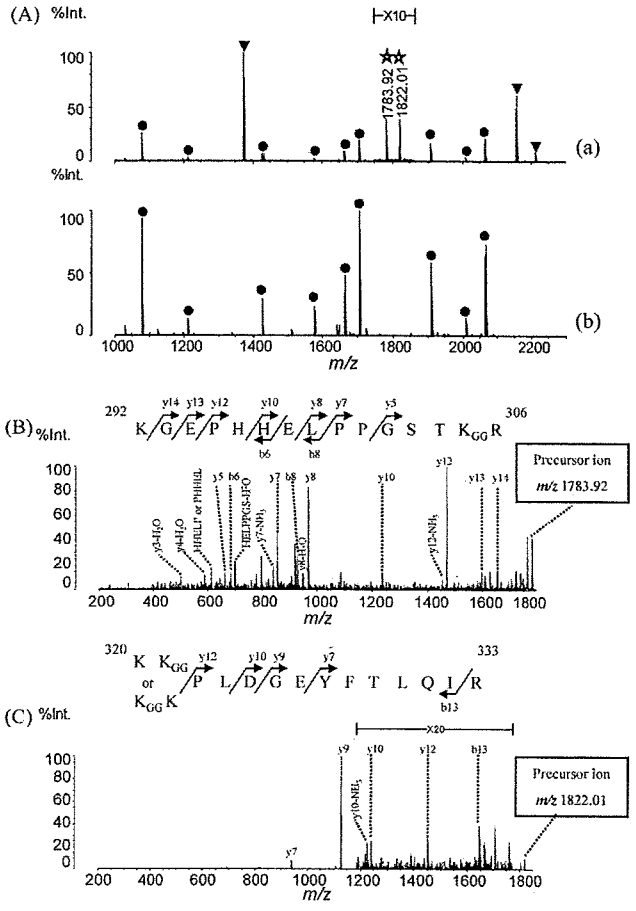

Fig. 7. MALDI-mass and -MS/MS spectra of tryptic digests of the affinity-purified p53 proteins. (A) The protein bands corresponding to (a) ubiquitinated p53 (p53-Ub) and (b) p53 proteins were excised individually. Each protein band was reduced and *S*-alkylated with iodeacetamide and then digested overnight with trypsin, and the digests were analyzed by MALDI-TOF MS. Filled circles and triangles indicate ions with the theoretical *m/z* values of tryptic digests of p53 and Me-Ub, respectively. Stars indicate probable tryptic peptides containing a GG-tag. MS/MS analyses were performed for the ions detected at *m/z* 1783.92 (B) and *m/z* 1822.01 (C) in (A). The observed fragment ions are indicated by the sequences shown. The subscript "GG" represents di-glycine residues from the C-terminal region of Ub.

bands were almost identical (A typical result is shown in Fig. 7A-a.). Peaks corresponding to tryptic peptides from both p53 and Me-Ub were detected in the mass spectrum (Fig. 7A-a). This result clearly indicated that Ub conjugation to p53 was generated in the insect cell-free protein synthesis system. The high molecular weight band (>160 kDa) detected in Fig. 6 was also analyzed by peptide mass fingerprinting, but we could not identify it (data not shown).

To identify the Ub-conjugation sites on p53, peaks corresponding to the tryptic digests were searched to find peptides with a GG-tag. Two peaks from the tryptic digests containing a GG-tag were detected at *m/z* 1783.92 and 1822.01 (Fig. 7A-a). These ions were further analyzed by MS/MS, which indicated that these ions were tryptic peptides having a GG-tag at Lys 305 (*m/z* 1783.92) and at Lys 320/321 (*m/z* 1822.01) (Fig. 7B and C).

4. Discussion

Ubiquitination is widely carried out in various cellular processes. Conjugation of Ub to target proteins can occur in both monomeric (mono-ubiquitination) and polymeric (poly-ubiquitination) forms. All seven internal Lys residues of Ub (Lys 6, 11, 27, 29, 33, 48, and 63) can be conjugated to Ub moieties to form poly-Ub chains (Ikeda and Dikic, 2008). In this study, we confirmed by MALDI-TOF MS and MALDI-QIT-TOF MS that Lys 29-, Lys 48-, and Lys 63-linked poly-Ub chain formation occurred in an insect cell-free protein synthesis system. Although it is unclear whether poly-Ub chains linked to other Lys residues are generated, and how many kinds of E2 Ub-conjugating enzymes and E3s exist in the insect cell-free protein synthesis system, the present results are sufficiently convincing to conclude that the insect cell-free protein synthesis system contains enzymatic activities capable of carrying out ubiquitination.

It is well accepted that ubiquitination plays a major role in p53 regulation. Although the C-terminal Lys residues (Lys 370, 372, 373, 381, 382, and 386) of p53 are known to be the major Ub acceptor sites for Mdm2-mediated ubiquitination (Rodriguez et al., 2000; Nakamura et al., 2000), the exact locations of the actual Ub acceptor sites of p53 are not fully defined. Although the possibility cannot be excluded that the Ub acceptor sites identified in this study may not accurately reflect the *in vivo* situation, we demonstrated that Lys 305 of p53 was one Ub acceptor site (Fig. 7B and Fig. 8). On the other hand, major Ub acceptor sites mediated by Mdm2 were not detected by MS analyses (Fig. 8), although Ub conjugations to p53 in the insect cell-free protein synthesis system were accelerated in the presence of Mdm2. One possible explanation for this is that it may be difficult to detect tryptic peptides from the C-terminal region of p53 by MALDI-TOF MS, because many short tryptic peptides are produced due to the existence of numerous Lys and Arg residues in this region (Fig. 8). It is not clear from the obtained results whether the Ub conjugations at Lys 305 and Lys 320/321 of p53 were mediated by Mdm2 or by another E3 in the insect cell-free protein synthesis system. The latter alternative is thought to be possible for the following reasons. First, it was recently demonstrated that E4F1, which is a zinc-finger protein, stimulates p53 ubiquitination on Lys 319 to Lys 321, and it was also demonstrated that these acceptor lysines are distinct from those targeted by Mdm2 (Cam et al., 2006) (Fig. 8). Second, Ub conjugation to p53 in the insect cell-free protein synthesis system was observed in the absence of Mdm2 (Fig. 4: lane 4).

We emphasize that Ub-conjugated p53 proteins were easily obtained using the insect cell-free protein synthesis system from the mRNA template transcribed from the corresponding cDNA. Thus this strategy should also be applicable to other cDNA resources. Although it is desirable that Ub conjugations occur effectively on target proteins without the addition of an exogenous

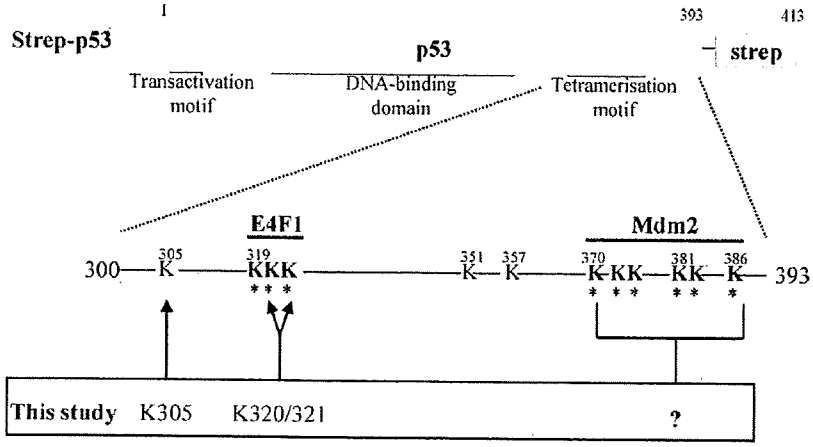

Fig. 8. Schematic representation of ubiquitination sites of p53. Asterisks indicate ubiquitination sites identified previously (Rodriguez et al., 2000; Nakamura et al., 2000; Cam et al., 2006). Arrows indicate Ub acceptor lysines determined in this study.

E3 protein, we think that it might be difficult because many E3s are tightly regulated by Ub-proteasome pathway or other PTMs (Meek and Knippschild, 2003). Further studies are necessary to elucidate general applicability of the insect cell-free protein synthesis system for *in vitro* ubiquitination assays. Quite recently, a method for *in vitro* analysis of ubiquitination based on wheat germ cell-free protein synthesis system and liminescent detection was reported (Takahashi et al., 2009). Although this strategy is effective for high-throughout detection of ubiquitination, it cannot be used to identify the exact location of the modification. We demonstrated that the ubiquitination sites generated *in vitro* could be identified by using the insect cell-free protein synthesis system and mass spectrometry. We think that it is critical to identify the precise structure and the exact location of the modification in PTM analysis. Thus, this insect cell-free protein synthesis system should prove to be a potent tool for *in vitro* ubiquitination assays of target proteins.

Acknowledgement

We thank Dr. Minoru Yamaguchi, Shimadzu Corporation, for the analysis of N-terminal amino acid sequences.

References

Cam, L.L., Linares, L.K., Paul, C., Julien, E., Lacroix, M., Hatchi, E., Triboulet, R., Bossis, G., Shmueli, A., Rodriguez, M.S., Coux, O., Sardet, C., 2006. E4F1 is an atypical ubiquitin ligase that modulates p53 effector functions independently of degradation. Cell 127, 775–788.

Chen, L., Marechal, V., Moreau, J., Levine, A.J., Chen, J., 1997. Proteolytic cleavage of the mdm2 oncoprotein during apoptosis. J. Biol. Chem. 272, 22966–22973.

Ciechanover, A., Digiuseppe, J.A., Bercovich, B., Orian, A., Richter, J.D., Schwartz, A.L., Brodeur, G.M., 1991. Degradation of nuclear oncoproteins by the ubiquitin system *in vitro*. Proc. Natl. Acad. Sci. U.S.A. 88, 139–143.

Ciechanover, A., 1998. The ubiquitin–proteasome pathway: on protein death and cell life. EMBO J. 17, 7151–7160.

Etlinger, J.D., Goldberg, A.L., 1977. A soluble ATP-dependent proteolysis system responsible for the degradation of abnormal proteins in reticulocytes. Proc. Natl. Acad. Sci. U.S.A. 74, 54–58.

Ezure, T., Suzuki, T., Higashide, S., Shintani, E., Endo, K., Kobayashi, S., Shikata, M., Ito, M., Tanimizu, K., Nishimura, O., 2006. Cell-free protein synthesis system prepared from insect cells by freeze–thawing. Biotechnol. Prog. 22, 1570–1577.

Ezure, T., Suzuki, T., Shikata, M., Ito, M., Ando, E., Nishimura, O., Tsunasawa, S., 2007. Expression of proteins containing disulfide bonds in an insect cell-free system and confirmation of their arrangements by MALDI-TOF mass spectrometry. Proteomics 7, 4424–4434.

Fang, S., Jensen, J.P., Ludwig, R.L., Vousden, K.H., Weissman, A.M., 2000. Mdm2 is a RING finger-dependent ubiquitin protein ligase for itself and p53. J. Biol. Chem. 275, 8945–8951.

Gururaja, T., Li, W., Noble, W.S., Payan, D.G., Anderson, D.C., 2003. Multiple functional categories of proteins identified in an in vitro cellular ubiquitin affinity extract using shotgun peptide sequencing. J. Proteome Res. 2, 394–404.

Haupt, Y., Maya, R., Kazaz, A., Oren, M., 1997. Mdm2 promotes the rapid degradation of p53. Nature 387, 296–299.

Hershko, A., Ciechanover, A., 1998. The ubiquitin system. Annu. Rev. Biochem. 67, 425–479.

Ikeda, F., Dikic, I., 2008. Atypical ubiquitin chains: new molecular signals. EMBO Rep. 9, 536–542.

Lai, Z., Ferry, K.V., Diamond, M.A., Wee, K.E., Kim, Y.B., Ma, J., Yang, T., Benfield, P.A., Copeland, R.A., Auger, K.R., 2001. Human mdm2 mediates multiple monoubiquitination of p53 by a mechanism requiring enzyme isomerization. J. Biol. Chem. 276, 31357–31367.

Meek, D.W., Knippschild, U., 2003. Posttranslational modification of MDM2. Mol. Cancer Res. 1, 1017–1026.

Nakamura, S., Roth, J.A., Mukhopadhyay, T., 2000. Multiple lysine mutations in the C-terminal domain of p53 interfere with Mdm2-dependent protein degradation and ubiquitination. Mol. Cell. Biol. 20, 9391–9398.

Peng, J., Schwartz, D., Elias, J.E., Thoreen, C.C., Cheng, D., Marsischky, G., Roelofs, J., Finley, D., Gygi, S.P., 2003. A proteomics approach to understanding protein ubiquitination. Nat. Biotechnol. 21, 921–926.

Pochampally, R., Fodera, B., Chen, L., Shao, W., Levine, E.A., Chen, A., 1998. A 60 kd MDM2 isoform is produced by caspase cleavage in non-apoptotic tumor cells. Oncogene 17, 2629–2636.

Pochampally, R., Fodera, B., Chen, L., Lu, W., Chen, J., 1999. Activation of an MDM2-specific caspase by p53 in the absence of apoptosis. J. Biol. Chem. 274, 15271–15277.

Rodriguez, M.S., Desterro, J.M.P., Lain, S., Lane, D.P., Hay, R.T., 2000. Multiple C-terminal lysine residues target p53 for ubiquitin-proteasome-mediated degradation. Mol. Cell. Biol. 20, 8458–8467.

Sakurai, N., Moriya, K., Suzuki, T., Sofuku, K., Mochiki, H., Nishimura, O., Utsumi, T., 2007. Detection of co- and post-translational protein N-myristoylation by metabolic labeling in an insect cell-free protein synthesis system. Anal. Biochem. 362, 236–244.

Suzuki, T., Ito, M., Ezure, T., Kobayashi, S., Shikata, M., Tanimizu, K., Nishimura, O., 2006a. Performance of expression vector, pTD1, in insect cell-free translation system. J. Biosci. Bioeng. 102, 69–71.

Suzuki, T., Ito, M., Ezure, T., Shikata, M., Ando, E., Utsumi, T., Tsunasawa, S., Nishimura, O., 2006b. N-Terminal protein modifications in an insect cell-free protein synthesis system and their identification by mass spectrometry. Proteomics 6, 4486–4495.

Suzuki, T., Ito, M., Ezure, T., Shikata, M., Ando, E., Utsumi, T., Tsunasawa, S., Nishimura, O., 2007. Protein prenylation in an insect cell-free protein synthesis system and identification of products by mass spectrometry. Proteomics 7, 1942–1950.

Takahashi, H., Nozawa, A., Seki, M., Shinozaki, K., Endo, Y., Sawasaki, T., 2009. A simple and high-sensitivity method for analysis of ubiquitination and polyubiquitination based on wheat cell-free protein synthesis. BMC Plant Biol. 9, 39.

Tomlinson, E., Palaniyappan, N., Tooth, D., Layfield, R., 2007. Methods for the purification of ubiquitinated proteins. Proteomics 7, 1016–1022.

Acta histochemica ▮ (▮▮▮▮) ▮▮▮–▮▮▮

ELSEVIER

Available online at www.sciencedirect.com

ScienceDirect

acta histochemica

www.elsevier.de/acthis

Molecular-assisted immunohistochemical optimization

Mohd Feroz Mohd Omar[a,b], Ning Huang[c,d], Keli Ou[c,d], Kun Yu[e], Thomas C. Putti[f], Hiroyuki Jikuya[c,d], Tetsuo Ichikawa[c,d], Osamu Nishimura[g], Patrick Tan[c,e,h,i], Manuel Salto-Tellez[a,f,*]

[a]*Oncology Research Institute, National University of Singapore, Singapore*
[b]*NUS Graduate School for Integrative Sciences and Engineering, Singapore*
[c]*Agenica Research Pte Ltd., Singapore*
[d]*Shimadzu (Asia Pacific) Pte Ltd., Singapore*
[e]*National Cancer Centre of Singapore, Singapore*
[f]*Department of Pathology, National University Hospital and National University of Singapore, 5, Lower Kent Ridge Road, 119074, Singapore*
[g]*Shimadzu Corporation, Nakagyo-ku, Kyoto, Japan*
[h]*Genome Institute of Singapore, Singapore*
[i]*Duke-NUS Graduate Medical School, Singapore*

Received 19 August 2008; received in revised form 6 May 2009; accepted 19 May 2009

KEYWORDS
Immunohistochemistry validation;
Molecular biology;
Molecular diagnostics;
Protein immunolocalization;
Antibody optimization

Summary

Immunohistochemistry (IHC) is an essential tool in diagnostic surgical pathology, allowing analysis of protein subcellular localization. The use of IHC by different laboratories has lead to inconsistencies in published literature for several antibodies, due to either interpretative (inter-observer variation) or technical reasons. These disparities have major implications in both clinical and research settings. In this study, we report our experience conducting an IHC optimization of antibodies against five proteins previously identified by proteomic analysis to be breast cancer biomarkers, namely 6PGL (PGLS), CAZ2 (CAPZA2), PA2G4 (EBP1) PSD2 and TKT. Large variations in the immunolocalizations and intensities were observed when manipulating the antigen retrieval method and primary antibody incubation concentration. However, the use of an independent molecular analysis method provided a clear indication in choosing the appropriate biologically and functionally relevant "staining pattern". Without this latter step, each of these contradictory results would have been *a priori* "technically acceptable" and would have led to different biological and functional interpretations of these proteins and potentially

*Corresponding author at: Department of Pathology, National University Hospital and National University of Singapore, 5, Lower Kent Ridge Road, 119074, Singapore. Tel.: +65 67724704; fax: +65 6778 0671.
E-mail address: patmst@nus.edu.sg (M. Salto-Tellez).

0065-1281/$ - see front matter
doi:10.1016/j.acthis.2009.05.010

Please cite this article as: Mohd Omar MF, et al. Molecular-assisted immunohistochemical optimization. Acta Histochem (2009), doi:10.1016/j.acthis.2009.05.010

different applications in a routine pathology setting. Thus, we conclude that full validation of immunohistochemical protocols for scientific and clinical use will require the incorporation of biological knowledge of the biomarker and the disease in question.

Introduction

Protein expression is the true "functional genomics" and knowledge of extracellular and/or subcellular localization is essential to elucidate the function of these proteins. Measuring the levels of protein expression and their putative correlation with RNA through gene expression are common activities in modern translational research. In the diagnostic arena, the use of immunohistochemistry (IHC) in addition to hematoxylin and eosin staining has been shown to increase diagnostic accuracy. Insights into the role of protein expression in disease progression and how this affects patient stratification and drug targeting, will ultimately lead to formulating the basis for personalized medicine (Douglas-Jones et al., 2005). The availability of tissues and the relative simplicity of IHC techniques make this a very widely used and accepted method for routine diagnostics.

IHC allows the *in situ* visualization of protein localization in specific cellular components, not only in the different regions of the tissue, but also within specific regions of cells. This is achieved by the precise interaction of an introduced antibody with a specific antigen, later visualized using a labelling system. For the most part, this technique is semi-quantitative and predominantly analyzed by a trained pathologist. Technically simple and relatively affordable, IHC is arguably the most widely used "molecular" analysis in research and diagnostic settings. Unfortunately, the wide use of this technique, which allows an "interpretative" approach to the analysis of results, also accounts for the known reported disparities in the results.

These disparities have been reported with regard to key molecular players in common cancers such as p53 in colorectal cancer (Soong et al., 1996) and estrogen receptor and c-erbB2 in breast cancer (Nedergaard et al., 1995; Perez et al., 2006) among many others which, in the case of breast cancer, may lead to suboptimal patient treatment. These apparent contradictions can be interpretative or technical. Classically, IHC interpretation is subjective (Biesterfeld et al., 1996), leading to inter-observer variability, which results in different observers scoring a particular case differently. Although systems for automated scoring of IHC are already commercially available, (Rojo et al., 2006) and some of them approved by the US Food and Drug Administration (FDA) for quantification of specific antibodies, these are not yet ready for universal use in research or diagnosis. Technical disparities are primarily attributed to differences in fixation protocol, IHC reagents, antigen retrieval protocols, antibody clone, concentrations and incubation times (Ainsworth et al., 2005; Boenisch, 2005; Goldstein et al., 2007; McCabe et al., 2005; McShane et al., 2000; Press et al., 1994, 2002; Ramos-Vara, 2005; Shi et al., 1997, 2001). These inconsistencies are a major hindrance in both clinical and research areas as they impact the interpretation of critical factors including clinical outcome, prognosis and potential biomarker discovery.

When working with a previously untested antibody, optimum experimental conditions must be established. To do so, several protocols are attempted to obtain 'correct' results based on the subjective criteria set by the researcher, such as immunolabelling intensity and absence of background 'noise'. This is, by definition, an arbitrary exercise, which may result in inter-observer variability. One approach to overcome this would be to introduce a 'standard' with which the immunolabelling could be compared. The approach to standardization could be done using either bench-based techniques or by *in silico* predictions (Guda, 2006; Horton et al., 2007; Nair and Rost, 2005; Nakai and Horton, 1999; Schneider and Fechner, 2004; Shatkay et al., 2007; Hoglund et al., 2006) based on the protein sequences. These approaches have been explored in considerable detail, however, the reliability of the predictions is variable.

In this study we examine the technical aspect of IHC disparity. We propose a workflow for systematic immunolabelling optimization (particularly applicable to previously untested primary antibodies), specifically protocols designed for immunolabelling optimization in formalin-fixed, paraffin wax-embedded (FFPE) material, based on knowledge of the subcellular localization by molecular techniques. In order to achieve this we investigated the use of an independent molecular technique and bioinformatics methods. Specifically, we apply such a methodological approach to five near-novel

Please cite this article as: Mohd Omar MF, et al. Molecular-assisted immunohistochemical optimization. Acta Histochem (2009), doi:10.1016/j.acthis.2009.05.010

antibodies, using a human breast carcinoma cell line, four different antigen retrieval methods and four different concentrations per antibody.

Material and methods

Cell culture and pellet formation

The human breast carcinoma cell line MCF-7 (ATCC: HTB-22) was obtained from the American Type Culture Collection (Rockville, MD, USA), work with this cell line was under NHG Domain-Specific Review Board approval (Reference DSRB-B/09/140). It was cultured in Eagle minimum essential medium, supplemented with 2 mM L-glutamine and Earle's balanced salts solution adjusted to contain 1.5 g/L sodium bicarbonate, 0.1 mM non-essential amino acids, 1 mM sodium pyruvate and 10% fetal bovine serum (Hyclone, Logan, UT, USA). The cells were cultured in a humidified incubator with 5% CO_2 at 37 °C. Cells were grown to confluence, washed in phosphate-buffered saline (PBS) and trypsinized for 5 min to detach cells. The cell suspension was transferred to a 15 mL tube, followed by centrifugation at 1000*g* for 5 min to obtain a cell pellet.

Formalin fixation and paraffin wax embedding (PPFE)

Cells were fixed in 10% neutral-buffered formalin for 30 min at room temperature. Cell pellets were then dehydrated with increasing concentrations of ethanol (70%, 80%, 90% and 100%) for 1 h each and then xylene for a final hour, with centrifugation at 200*g* for 3 min between each step. The cells were then covered in paraffin wax blended with synthetic polymers (congealing temperature 58 °C) (BDH Chemicals Ltd., Poole, Dorset, England) and left overnight at 60 °C. These pellets were then placed into conventional paraffin wax embedding cassettes for sectioning.

Sectioning and immunocytochemistry

The FFPE blocks were sectioned at 4 μm thick and sections mounted on Matsunami adhesive silane (MAS)-coated glass microslides (Superfrost, Matsunami, Tokyo, Japan) and dried overnight at 37 °C. Paraffin wax was removed by three washes in xylene, and the tissue rehydrated in decreasing concentrations of ethanol (100%, 90% and 70%) and water for 5 min each.

The optimization experiments for the five antibodies (Table 1) involved four different antigen retrieval protocols for each antibody. These were performed by immersion of the sections in one of four different buffers (citrate buffer (PC), Tris–EDTA (EDTA), Dako pH 6.0 antigen retrieval buffer (DK6) or Dako pH 9.0 antigen retrieval buffer (DK9) and heating in a pressure cooker (T/T Mega, Milestone) at 120 °C for 5 min. This was followed with incubation with peroxidase block solution (ready-to-use from Dako, Glostrup, Denmark), followed by three rinses in washing buffer (PBS buffer containing 0.1% Tween 20). Five different primary antibodies were used in the study (Table 1), incubated at four different dilutions per antigen retrieval method, namely 1/50, 1/100, 1/200 and 1/400 (diluted with Dako antibody diluent), so that with the variation in antigen retrieval, there were 16 protocols used for each antibody. These five near-novel antibodies (either unused or seldom used for immunohistochemistry previously, and thus with no reliable previous indication of appropriate protocol or immunolabelling distribution) were used in the context of the validation in human clinical samples of a proteomics study in breast cancer cell lines (Ou et al., 2008).

Table 1. Antibody information with chosen protocol for each antibody.

Protein target	Full name	Antibody source	Optimised protocol[a]
6PGL (PGLS)	6-Phosphogluconolactonase	Customized by BioGenes (Berlin, Germany)	EDTA 1/50
CAZ2 (CAPZA2)	F-actin capping protein alpha-2 subunit	Customized by BioGenes (Berlin, Germany)	DK6 1/400
PA2G4 (EBP1)	Proliferated associated protein-2G4	Upstate (Lake Placid, NY, USA)	DK9 1/50
PSD2	26S proteasome non-ATPase regulatory subunit 2	Customized by BioGenes (Berlin, Germany)	DK9 1/200
TKT	Transketolase	Customized by BioGenes (Berlin, Germany)	DK9 1/50

[a]Chosen protocol is the protocol that best reflects the expected results based on the western blots.

Please cite this article as: Mohd Omar MF, et al. Molecular-assisted immunohistochemical optimization. Acta Histochem (2009), doi:10.1016/j.acthis.2009.05.010

Primary antibodies were incubated with sections overnight at room temperature, followed by three rinses in washing buffer. The peroxidase-labelled secondary antibody (EnVision+ kit, Dako, Glostrup, Denmark), prepared according to manufacturer's instructions, was allowed to incubate with the sections for 30 min at room temperature, again followed by three rinses in washing buffer. Antibody binding was detected by a peroxidase-3,3'-diaminobenzidine-based detection system (EnVision+ kit, Dako, Glostrup, Denmark), employed according to kit instructions. The slides were then counterstained with Gill's hematoxylin (Merck Pte. Ltd., Singapore). Finally the slides were dehydrated in increasing concentrations of ethanol (70%, 90% and 100%) for 5 min each, allowed to dry and mounted with a coverslip (Menzel-Gläser, Braunschweig, Germany) using DPX mountant (Fluka, Sigma-Aldrich, Buchs, Switzerland).

Protein extraction and western blot analysis

Protein extraction was performed using the ProteoExtract® Subcellular Proteome Extraction Kit (Calbiochem, EMD Chemicals, Inc., La Jolla, CA, USA), employed according to kit instructions. Briefly, this kit allows the fractionated extraction of the different cellular components, i.e. cytosolic protein, membrane/organelle protein and nucleic protein extracts, based on differing solubilities. Determination of protein concentrations was performed using the Coomassie blue (Bradford) protein assay kit (Pierce, Rockford, IL, USA), according to manufacturer's intructions. SDS-PAGE was performed using a 10% acrylamide gel under standard conditions. A semi-dry transfer was then performed onto a PVDF membrane (Bio-Rad Laboratories (Singapore) Pte. Ltd.) at 15 V for 40 min. The membranes were then blocked with 5% skim milk (Fluka, Sigma-Aldrich, Buchs, Switzerland) in washing buffer. The blots were probed with the antibodies shown in Table 1 at room temperature for 1 h. This was followed by incubation with the secondary antibody (ECL rabbit IgG, horseradish peroxidase-linked whole Ab, GE Pacific Pte Ltd., Singapore) diluted 1/50000 in washing buffer for 1 h. Detection was performed by chemiluminescence using the ECL advance detection kit (GE Pacific Pte Ltd., Singapore), carried out according to kit instructions. The reactivity was visualized on a VersaDoc 5000 (Bio-Rad Laboratories (Singapore) Pte. Ltd.) and analysis of banding using the Quantity One software (Bio-Rad Laboratories (Singapore) Pte. Ltd.).

Scoring of immuncytochemical labelling and comparison to western blot results

Immunolabelling of paraffin wax-embedded sections was scored according to intensity: 0 (negative – no immunolabelling), 1 (mild immunopositivity), 2 (moderate immunopositivity) and 3 (strong immunopositivity), and subcellular localization (nuclear or cytoplasmic). Scoring was performed by a trained scientist (MFMO) and confirmed by a qualified pathologist (MST). To avoid the consideration of non-specific labelling, and to make sure that no false positive results were included in our analysis, only intensities of 2 and 3 were accepted as positive for the purpose of this analysis. Based on the observations, the results were classified into five different categories: (1) even nuclear and cytoplasmic staining, where the intensity of immunolabelling of the nuclear and cytoplasmic components of the cell were both positive and even; (2) primarily nuclear staining, where the nuclear component of the cell was more intensely immunopositive than the cytoplasmic component; (3) primarily cytoplasmic staining, where the cytoplasmic component of the cell was more intensely immunopositive than the nuclear component; (4) variability in nuclear staining, where the immunolabelling in the nucleus varied from cell to cell within the sample; (5) negative for staining, where both the nuclear and cytoplasmic components were unlabelled. Immunopositivity of the western blots are listed as cytoplasmic, membrane/organelle and nucleic, based on the fractionation.

Bioinformatic prediction of protein localization

In order to predict protein localization, three *in silico* animal protein prediction programs were used, specifically Wolf pSORT (Horton et al., 2007), SherLoc (Shatkay et al., 2007) and MultiLoc (Hoglund et al., 2006). Briefly these techniques use prediction algorithms to predict localization of a protein based on structural motifs and signaling sequences. This is achieved by the use of machine learning techniques and the comparison of the protein's sequence against a panel of known proteins from a database (Hoglund et al., 2006; Horton et al., 2007; Shatkay et al., 2007). FASTA format sequences were used for input into the programs. The protein accession numbers for the five protein targets in this study are as follows: O95336 (6PGL), P47755 (CAZA2), Q9UQ80 (PA2G4), Q9BQI7 (PSD2) and P29401 (TKT).

Please cite this article as: Mohd Omar MF, et al. Molecular-assisted immunohistochemical optimization. Acta Histochem (2009), doi:10.1016/j.acthis.2009.05.010

Results

Table 2 summarises the results for all antibody concentrations and antigen retrieval variations of the IHC protocols. Figure 1 illustrates a summary of these results and depicts all the possible immunolabelling variations observed using the five different antibodies. This illustrates the different results that are possible when using a single antibody with different antigen retrieval methods and antibody concentrations. The IHC results indicate a large variability is possible for all the antibodies tested, with immunolabelling ranging from no labelling to either predominantly nuclear or cytoplasmic labelling for any given antibody. It should be noted that not all the antibodies exhibited all immunolabelling

Table 2. Immunolabelling patterns seen using the different protocols.

Antibody target	Dilution of primary antibody	Antigen retrieval using DK6	Antigen retrieval using DK9	Antigen retrieval using EDTA	Antigen retrieval using PC
6PGL	1/50	Primarily cytoplasmic	Primarily cytoplasmic	**Primarily cytoplasmic**	Even nuclear and cytoplasmic
	1/100	Primarily cytoplasmic	Primarily cytoplasmic	Primarily cytoplasmic	Primarily cytoplasmic
	1/200	Primarily cytoplasmic	Primarily cytoplasmic	Primarily cytoplasmic	Variability in nuclear staining
	1/400	Primarily cytoplasmic	Primarily cytoplasmic	Negative for staining	Variability in nuclear staining
CAZ2	1/50	Even nuclear and cytoplasmic	Variability in nuclear staining	Primarily nuclear	Even nuclear and cytoplasmic
	1/100	Even nuclear and cytoplasmic	Variability in nuclear staining	Primarily nuclear	Even nuclear and cytoplasmic
	1/200	Primarily cytoplasmic	Variability in nuclear staining	Variability in nuclear staining	Primarily nuclear
	1/400	**Primarily cytoplasmic**	Negative for staining	Primarily nuclear	Negative for staining
PA2G4	1/50	Even nuclear and cytoplasmic	**Even nuclear and cytoplasmic**	Variability in nuclear staining	Primarily nuclear
	1/100	Variability in nuclear staining	Even nuclear and cytoplasmic	Variability in nuclear staining	Primarily nuclear
	1/200	Primarily cytoplasmic	Even nuclear and cytoplasmic	Variability in nuclear staining	Even nuclear and cytoplasmic
	1/400	Primarily cytoplasmic	Even nuclear and cytoplasmic	Primarily cytoplasmic	Even nuclear and cytoplasmic
PSD2	1/50	Variability in nuclear staining	Even nuclear and cytoplasmic	Primarily cytoplasmic	Primarily nuclear
	1/100	Variability in nuclear staining	Even nuclear and cytoplasmic	Variability in nuclear staining	Primarily nuclear
	1/200	Primarily nuclear	**Even nuclear and cytoplasmic**	Variability in nuclear staining	Primarily nuclear
	1/400	Primarily nuclear	Primarily nuclear	Variability in nuclear staining	Primarily nuclear
TKT	1/50	Primarily nuclear	**Even nuclear and cytoplasmic**	Primarily nuclear	Primarily nuclear
	1/100	Even nuclear and cytoplasmic	Primarily nuclear	Primarily nuclear	Primarily nuclear
	1/200	Even nuclear and cytoplasmic	Primarily nuclear	Primarily nuclear	Primarily nuclear
	1/400	Negative for staining	Primarily nuclear	Primarily nuclear	Negative for staining

The optimal protocol for each antibody, based on its correspondence with the western blot results, are highlighted in bold.

Please cite this article as: Mohd Omar MF, et al. Molecular-assisted immunohistochemical optimization. Acta Histochem (2009), doi:10.1016/j.acthis.2009.05.010

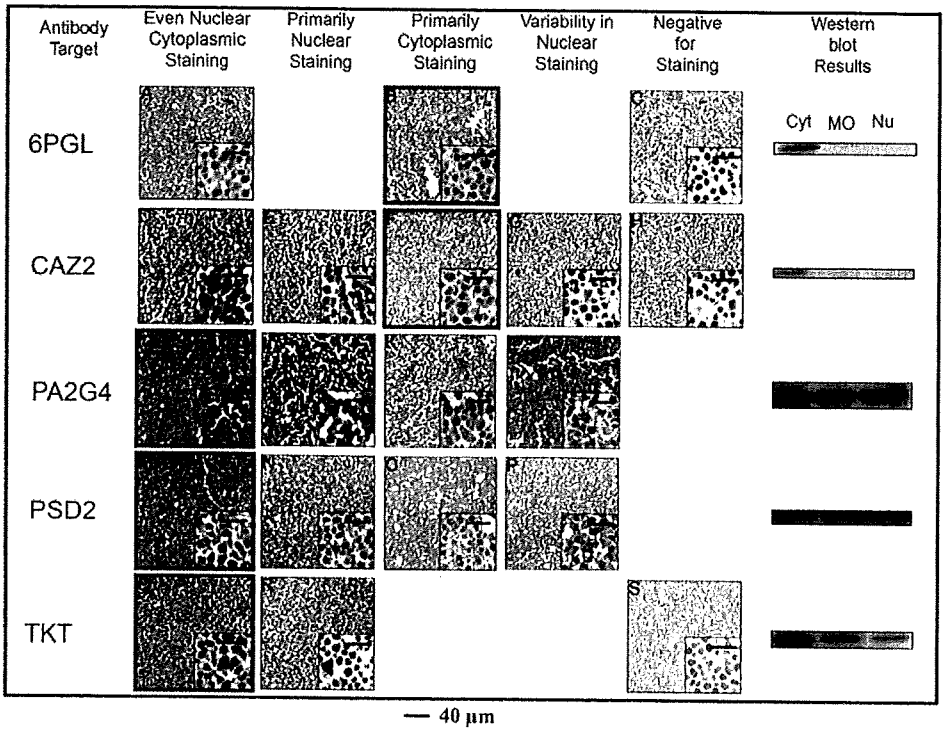

Figure 1. Variation in antibody immunolabelling intensity and localization. Horizontal rows correspond to the antibodies against the different proteins, while vertical columns show the different localization patterns. The results that match the western blot observation are shown with a blue border. The results were categorized into five different possible observations. As shown, the possible outcomes were dependant on the antibody used, i.e. only certain immunolabelling categories were observed for each of the antibodies. The larger image was taken at 100× magnification, whole the panel image was taken at 400× magnification. The protocols used in each case are shown below (antigen retrieval methods followed by the antibody dilution factor) (A) PC, 1/50, (B) EDTA 1/50, (C) EDTA 1/400, (D) PC 1/50, (E) EDTA 1/50, (F) DK6 1/400, (G) DK9 1/50, (H) DK9 1/400, (I) DK9 1/50, (J) PC 1/100, (K) DK6 1/400, (L) EDTA 1/50, (M) DK9 1/200, (N) PC 1/400, (O) EDTA 1/50, (P) EDTA 1/200, (Q) DK9 1/50, (R) DK9 1/400, (S) PC 1/400; PC-citrate buffer, EDTA-Tris-EDTA, DK6-DAKP pH6.0, DK9-DAKO pH 9.0, Cyt – cytosolic fraction, MO – membrane/organelle fraction, Nu – nucleic protein extract.

patterns, for example, CAZ2 exhibits all the immunolabelling variations, while 6PGL and TKT labelled in only three different patterns.

The different antibodies also exhibited varying protein localization patterns and immunolabelling intensities on western blots (Figure 1). 6PGL and CAZ2 labelled only cytoplasmic components, while PA2G4, PSD2 and TKT showed strong labelling in all cellular fractions. The most biologically appropriate immunolocalisation using IHC was judged to be that which corresponded to the western blot result. The IHC results that most closely corresponded to the western blot observations are framed in blue in Figure 1 and highlighted in Table 2. The optimized final protocol for each antibody was different; hence there was no single protocol that was appropriate for all antibodies in the study.

A direct comparison of the three bioinformatics methods used is rather difficult, owing to the different prediction output formats. Table 3 summarises these results, with a standardization of terms when necessary. An overall analysis does, however, reveal that there is no robust agreement between the subcellular localization predictions of the three bioinformatics programs, nor was there an unequivocal correlation of any of the programs with the western blot results.

Discussion

Cell lines serve as the ideal source material for antibody optimization as the derived pellet is a biologically homogenous sample, minimizing the intrinsic variability of the optimization exercise. Cells are relatively easy to manipulate and are a renewable source for multiple optimization and experimentation. For the experimental design, we chose a representative cell line, MCF-7, obtained

Please cite this article as: Mohd Omar MF, et al. Molecular-assisted immunohistochemical optimization. Acta Histochem (2009), doi:10.1016/j.acthis.2009.05.010

Table 3. Comparison of western blot results to WoLF pSORT, SherLoc and MultiLoc2 protein localization predictions.

Antibody	Western blot localization	WoLF pSORT	SherLoc	MultiLoc2
6PGL (PGLS)	Primarily cytoplasmic	Extr: 14.0 Cyto and Nu: 7.7 Nu: 5.5 Mito: 5.0 Cyto and Pero: 4.7 Cyto: 4.5	Cyto: 0.36	Mito: 0.59 Cyto: 0.25 Nu: 0.11 Extr: 0.05
CAZ2 (CAPZA2)	Primarily cytoplasmic	Cyto: 20.5 Cyto and Nu: 14.5 Nu: 5.5 Cysk: 5.0	Cyto: 0.72	Cyto: 0.83 Nu: 0.16 Mito: 0.0 Extr: 0.0
PA2G4 (EBP1)	Even nuclear and cytoplasmic	Nu: 21.5 Cyto and Nu: 15.0 Cyto: 7.5	Nu: 0.93	Cyto: 0.53 Nu: 0.47 Mito: 0.0 Extr: 0.0
PSD2	Even nuclear and cytoplasmic	Plas: 23.0 Er: 6.0	Nu: 0.49	Cyto: 0.78 Nu: 0.21 Mito: 0.01 Extr: 0.0
TKT	Even nuclear and cytoplasmic	Cyto: 18.0 Cytoand Nu: 15.3 Cytoand Plas: 10.2 Nu: 7.5 Er: 3.0	Cyto: 1.0	Cyto: 0.73 Nu: 0.24 Mito: 0.02 Extr: 0.0

Results are shown as rank values that indicate favorability to a specific localization. Higher values indicate a higher likelihood of occurrence at the specific localization site. WoLF pSort and MultLoc2 provide several probable locations for a protein, while SherLoc displays only the most likely localization site. Nu – nuclear, Pero – peroxisomal, Cyto – cytoplasmic, Er – endoplasmic reticulum, Cysk – cytoskeleton, Extr – extracellular, Mito – mitochondrial, Plas-plasma membrane.

from the pleural effusion of a patient with metastatic breast carcinoma (Soule et al., 1973). It is a well characterized estrogen receptor (ER) positive cell line, which is a standard model for the study of breast cancer in laboratories around the world (Lau et al., 2006; Levenson and Jordan, 1997). The cells were formalin-fixed and paraffin wax-embedded to emulate the conditions faced during routine processing and embedding of clinical samples available in conventional pathology departments worldwide. It should be noted that the protein extraction and subsequent western blots were intentionally performed on fresh cells, so as not to introduce any factors that may cause degradation to the protein (Boenisch, 2006). Subsequently, the various optimization protocols were performed using the FFPE material. This approach allowed us to select the protocol for use with FFPE tissue that most closely represented the native state of the protein localization as indicated by the western blots.

As seen in Figure 1 and Table 2, the variation in the immunolabelling patterns of each antibody is very apparent, indicating that the results of any one protocol may be contradictory to the actual protein localization and concentration, and that this is dependent on the antigen retrieval method and primary antibody concentration. The interpretation of this substantial variability for any given antibody ranges from assuming that a protein is not present in a tumor to accepting a functional overexpression of the same protein. This would be very misleading to a researcher and the implication of the incorrect localization patterns would be quite severe in a clinical setting, where inconsistencies could result in incorrect diagnosis, prognosis and treatment.

The introduction of protein from fresh cells and the fractionated western blot analysis was essential in elucidating the biologically correct immunolocalisation pattern, including the subcellular localization which, in itself, dictates the precise functionality of the protein, with the understanding that for practical purposes, cytoplasmic and membranous immunopositivity in the western blot corresponds to general cytoplasmic immunopositivity in IHC.

It should be noted that for each primary antibody, more than one IHC protocol resulted in the

Please cite this article as: Mohd Omar MF, et al. Molecular-assisted immunohistochemical optimization. Acta Histochem (2009), doi:10.1016/j.acthis.2009.05.010

immunolocalisation of the protein consistent with western blot results (Table 1). The number of consistent localizations varied from two different protocols for CAZ2 (primarily cytoplasmic) to as many as 12 different protocols for 6PGL (primarily cytoplasmic). The choice of the most appropriate protocol, consistent with the western blot results, was made by also taking into account the intensity of the IHC labeling; that is, where the immunolabelling intensity values were high, between 2 and 3. An interesting observation is that changes in antigen retrieval buffer appeared to play more of a crucial role in apparent protein subcellular localization rather than primary antibody concentration, and therefore should be of primary concern in an optimization protocol. Without the use of the western blot in an optimization protocol a scientist may have regarded the antibody as optimized with any one of the protocols used, potentially resulting in a drastic difference from actual biological localization of a studied protein. This can be illustrated by the known phenomenon of protein mis-localization and its relevance in protein function. For example, we have shown that subcellular localization of RUNX3 is tightly related to the development of breast cancer (Ito et al., 2005). Others have established its importance in BRCA1 and breast cancer (Rodriguez et al., 2004), in acute promyelocytic leukemia cells that express chimeric RARα fusion proteins (Dong et al., 2004), in human thyroid cancer and p27 (kip1) expression by phosphorylation-dependent cytoplasmic sequestration (Motti et al., 2005) and SRC-1 androgen receptor-dependent nuclear sequestration in prostate cancer (Nazareth et al., 1999), among others.

It is well known that cell lines are prone to genotypic and phenotypic drift during culture, causing the appearance of heterogeneous subpopulations (Burdall et al., 2003; Maitra et al., 2005). Indeed, previous studies have shown that the MCF-7 cell line has shown a high level of clonal variation, including both phenotypic and karyotypic variation (Bahia et al., 2002; Burow et al., 1998; Nugoli et al., 2003; Osborne et al., 1987). This indicates the importance of linking the appearance in western blots and IHC with the knowledge of protein function using a similar passage number and/or origin.

As part of our antibody optimization experiments, we only included the more common and easily altered variables – antigen retrieval method and primary antibody concentration. However, there may be occasions in which adequate results are not obtained by altering these variables alone and then other methodological aspects should be considered, such as, the length of antigen retrieval, the use of different antibody clones detecting different epitopes in the same protein or the molecular optimization using a different cell line. To maintain relative simplicity in the optimization process, we recommend these steps only if necessary, i.e. these factors represent a second line set of variables in the optimization process.

A potential barrier to the use of the approach described here in clinical pathology laboratories is the lack of available cell culture facilities in these routine settings. However, we believe that the cell pelleting protocol described in this paper is simple enough to be carried out in any cytopathology facility and, hence, all that is required from clinical laboratories is to contact research laboratories to acquire the prepared cells with the stipulated characteristics.

In any case, we believe that the lack of access to cell lines and molecular techniques in general by immunohistochemistry-based laboratories may be mitigated, at least in part, in the future. This is so because of the need to combine morphology-based diagnostics with molecular diagnostics in a single laboratory operation. This model on combined morpho-molecular diagnostics will not only be of advantage to the patient and to the pathologist (Salto-Tellez, 2007), but will also make combined approaches for optimization such as the one we are proposing here much more readily available.

As indicated in the small comparative analysis described here, the variation between several well-regarded bioinfomatic predictors of subcellular localization indicate that more work is still necessary before these are readily applied to IHC validation, particularly in the context of clinical immunohistochemistry.

In summary, we have shown that a systematic protocol for IHC optimization, taking into account a parallel mode of protein detection and the functional knowledge of the individual proteins, may improve the consistency of results between different laboratories studying the same proteins and using different antibodies and protocols (McShane et al., 2000; Mengel et al., 2002; Parker et al., 2002; von Wasielewski et al., 2002). Overall, this may also contribute to improving the knowledge of novel proteins in clinical samples and human diseases. With the existing methodology, our study suggests that, to date, the 'standard' used for optimization should preferably be derived by bench-based experiments, rather than bioinformatic prediction techniques.

References

Ainsworth R, Bartlett JM, Going JJ, Mallon EA, Forsyth A, Richmond J, et al. IHC for Her2 with CBE356 antibody

Please cite this article as: Mohd Omar MF, et al. Molecular-assisted immunohistochemical optimization. Acta Histochem (2009), doi:10.1016/j.acthis.2009.05.010

is a more accurate predictor of Her2 gene amplification by FISH than HercepTest in breast carcinoma. J Clin Pathol 2005;58:1086–90.

Bahia H, Ashman JN, Cawkwell L, Lind M, Monson JR, Drew PJ, et al. Karyotypic variation between independently cultured strains of the cell line MCF-7 identified by multicolour fluorescence in situ hybridization. Int J Oncol 2002;20:489–94.

Biesterfeld S, Veuskens U, Schmitz FJ, Amo-Takyi B, Bocking A. Interobserver reproducibility of immunocytochemical estrogen- and progesterone receptor status assessment in breast cancer. Anticancer Res 1996;16:2497–500.

Boenisch T. Effect of heat-induced antigen retrieval following inconsistent formalin fixation. Appl Immunohistochem Mol Morphol 2005;13:283–6.

Boenisch T. Heat-induced antigen retrieval: what are we retrieving? J Histochem Cytochem 2006;54:961–4.

Burdall SE, Hanby AM, Lansdown MR, Speirs V. Breast cancer cell lines: friend or foe? Breast Cancer Res 2003;5:89–95.

Burow ME, Weldon CB, Tang Y, Navar GL, Krajewski S, Reed JC, et al. Differences in susceptibility to tumor necrosis factor alpha-induced apoptosis among MCF-7 breast cancer cell variants. Cancer Res 1998;58: 4940–6.

Dong S, Stenoien DL, Qiu J, Mancini MA, Tweardy DJ. Reduced intranuclear mobility of APL fusion proteins accompanies their mislocalization and results in sequestration and decreased mobility of retinoid X receptor alpha. Mol Cell Biol 2004;24:4465–75.

Douglas-Jones A, Shah V, Morgan J, Dallimore N, Rashid M. Observer variability in the histopathological reporting of core biopsies of papillary breast lesions is reduced by the use of immunohistochemistry for CK5/6, calponin and p63. Histopathology 2005;47:202–8.

Goldstein NS, Hewitt SM, Taylor CR, Yaziji H, Hicks DG. Recommendations for improved standardization of immunohistochemistry. Appl Immunohistochem Mol Morphol 2007;15:124–33.

Guda C. pTARGET: a web server for predicting protein subcellular localization. Nucleic Acids Res 2006;34: W210–3.

Hoglund A, Donnes P, Blum T, Adolph H-W, Kohlbacher O. MultiLoc: prediction of protein subcellular localization using N-terminal targeting sequences, sequence motifs and amino acid composition. Bioinformatics 2006;22:1158–65.

Horton P, Park KJ, Obayashi T, Fujita N, Harada H, Adams-Collier CJ, et al. WoLF PSORT: protein localization predictor. Nucleic Acids Res 2007;35:W585–7.

Ito K, Liu Q, Salto-Tellez M, Yano T, Tada K, Ida H, et al. RUNX3, a novel tumor suppressor, is frequently inactivated in gastric cancer by protein mislocalization. Cancer Res 2005;65:7743–50.

Lau QC, Raja E, Salto-Tellez M, Liu Q, Ito K, Inoue M, et al. RUNX3 is frequently inactivated by dual mechanisms of protein mislocalization and promoter hypermethylation in breast cancer. Cancer Res 2006; 66:6512–20.

Levenson AS, Jordan VC. MCF-7: the first hormone-responsive breast cancer cell line. Cancer Res 1997; 57:3071–8.

Maitra A, Arking DE, Shivapurkar N, Ikeda M, Stastny V, Kassauei K, et al. Genomic alterations in cultured human embryonic stem cells. Nat Genet 2005;37: 1099–103.

McCabe A, Dolled-Filhart M, Camp RL, Rimm DL. Automated quantitative analysis (AQUA) of in situ protein expression, antibody concentration, and prognosis. J Natl Cancer Inst 2005;97:1808–15.

McShane LM, Aamodt R, Cordon-Cardo C, Cote R, Faraggi D, Fradet Y, et al. Reproducibility of p53 immunohistochemistry in bladder tumors. National Cancer Institute, Bladder Tumor Marker Network. Clin Cancer Res 2000;6:1854–64.

Mengel M, Wasielewski R, Wiese B, Rudiger T, Muller-Hermelink HK, Kreipe H. Inter-laboratory and inter-observer reproducibility of immunohistochemical assessment of the Ki-67 labelling index in a large multicentre trial. J Pathol 2002;198:292–9.

Motti ML, Califano D, Troncone G, Marco C, Migliaccio I, Palmieri E, et al. Complex regulation of the cyclin-dependent kinase inhibitor p27kip1 in thyroid cancer cells by the PI3K/AKT pathway: regulation of p27kip1 expression and localization. Am J Pathol 2005;166: 737–49.

Nair R, Rost B. Mimicking cellular sorting improves prediction of subcellular localization. J Mol Biol 2005; 348:85–100.

Nakai K, Horton P. PSORT: a program for detecting sorting signals in proteins and predicting their subcellular localization. Trends Biochem Sci 1999;24: 34–6.

Nazareth LV, Stenoien DL, Bingman WE, James aJ, Wu C, Zhang Y, et al. C619Y mutation in the human androgen receptor causes inactivation and mislocalization of the receptor with concomitant sequestration of SRC-1 (steroid receptor coactivator 1). Mol Endocrinol 1999; 13:2065–75.

Nedergaard L, Haerslev T, Jacobsen GK. Immunohistochemical study of estrogen receptors in primary breast carcinomas and their lymph node metastases including comparison of two monoclonal antibodies. APMIS 1995;103:20–4.

Nugoli M, Chuchana P, Vendrell J, Orsetti B, Ursule L, Nguyen C, et al. Genetic variability in MCF-7 sublines: evidence of rapid genomic and RNA expression profile modifications. BMC Cancer 2003;3:13.

Osborne CK, Hobbs K, Trent JM. Biological differences among MCF-7 human breast cancer cell lines from different laboratories. Breast Cancer Res Treat 1987;9:111–21.

Ou K, Yu K, Kesuma D, Hooi M, Huang N, Chen W, et al. Novel breast cancer biomarkers identified by integrative proteomic and gene expression mapping. J Proteome Res 2008;7:1518–28.

Parker RL, Huntsman DG, Lesack DW, Cupples JB, Grant DR, Akbari M, et al. Assessment of interlaboratory variation in the immunohistochemical determination

Please cite this article as: Mohd Omar MF, et al. Molecular-assisted immunohistochemical optimization. Acta Histochem (2009), doi:10.1016/j.acthis.2009.05.010

of estrogen receptor status using a breast cancer tissue microarray. Am J Clin Pathol 2002;117:723–8.
Perez EA, Suman VJ, Davidson NE, Martino S, Kaufman PA, Lingle WL, et al. HER2 testing by local, central, and reference laboratories in specimens from the North Central Cancer Treatment Group N9831 intergroup adjuvant trial. J Clin Oncol 2006;24:3032–8.
Press MF, Hung G, Godolphin W, Slamon DJ. Sensitivity of HER-2/neu antibodies in archival tissue samples: potential source of error in immunohistochemical studies of oncogene expression. Cancer Res 1994;54: 2771–7.
Press MF, Slamon DJ, Flom KJ, Park J, Zhou JY, Bernstein L. Evaluation of HER-2/neu gene amplification and overexpression: comparison of frequently used assay methods in a molecularly characterized cohort of breast cancer specimens. J Clin Oncol 2002;20: 3095–105.
Ramos-Vara JA. Technical aspects of immunohistochemistry. Vet Pathol 2005;42:405–26.
Rodriguez JA, Au WW, Henderson BR. Cytoplasmic mislocalization of BRCA1 caused by cancer-associated mutations in the BRCT domain. Exp Cell Res 2004; 293:14–21.
Rojo MG, Garcia GB, Mateos CP, Garcia JG, Vicente MC. Critical comparison of 31 commercially available digital slide systems in pathology. Int J Surg Pathol 2006;14:285–305.
Salto-Tellez MA. Case for integrated morphomolecular diagnostic pathologists. Clin Chem 2007;53:1188–90.
Schneider G, Fechner U. Advances in the prediction of protein targeting signals. Proteomics 2004;4:1571–80.
Shatkay H, Hoglund A, Brady S, Blum T, Donnes P, Kohlbacher O. SherLoc: high-accuracy prediction of protein subcellular localization by integrating text and protein sequence data. Bioinformatics 2007;23: 1410–7.
Shi S-R, Cote RJ, Taylor CR. Antigen retrieval immunohistochemistry: past, present, and future. J Histochem Cytochem 1997;45:327–44.
Shi S-R, Cote RJ, Taylor CR. Antigen retrieval techniques: current perspectives. J Histochem Cytochem 2001;49: 931–8.
Soong R, Robbins PD, Dix BR, Grieu F, Lim B, Knowles S, et al. Concordance between p53 protein overexpression and gene mutation in a large series of common human carcinomas. Hum Pathol 1996;27:1050–5.
Soule HD, Vazguez J, Long A, Albert S, Brennan MA. Human cell line from a pleural effusion derived from a breast carcinoma. J Natl Cancer Inst 1973;51:1409–16.
Wasielewski R, Mengel M, Wiese B, Rudiger T, Muller-Hermelink HK, Kreipe H. Tissue array technology for testing interlaboratory and interobserver reproducibility of immunohistochemical estrogen receptor analysis in a large multicenter trial. Am J Clin Pathol 2002;118:675–82.

Please cite this article as: Mohd Omar MF, et al. Molecular-assisted immunohistochemical optimization. Acta Histochem (2009), doi:10.1016/j.acthis.2009.05.010

Ritchie et al. BMC Medicine 2010, 8:13
http://www.biomedcentral.com/1741-7015/8/13

BMC Medicine

RESEARCH ARTICLE Open Access

Reduced levels of hydroxylated, polyunsaturated ultra long-chain fatty acids in the serum of colorectal cancer patients: implications for early screening and detection

Shawn A Ritchie[1*], Pearson WK Ahiahonu[1], Dushmanthi Jayasinghe[1], Doug Heath[1], Jun Liu[1], Yingshen Lu[1], Wei Jin[1], Amir Kavianpour[1], Yasuyo Yamazaki[1], Amin M Khan[1], Mohammad Hossain[1], Khine Khine Su-Myat[1], Paul L Wood[1], Kevin Krenitsky[2], Ichiro Takemasa[3], Masakazu Miyake[3], Mitsugu Sekimoto[3], Morito Monden[3], Hisahiro Matsubara[4], Fumio Nomura[5], Dayan B Goodenowe[1]

Abstract

Background: There are currently no accurate serum markers for detecting early risk of colorectal cancer (CRC). We therefore developed a non-targeted metabolomics technology to analyse the serum of pre-treatment CRC patients in order to discover putative metabolic markers associated with CRC. Using tandem-mass spectrometry (MS/MS) high throughput MS technology we evaluated the utility of selected markers and this technology for discriminating between CRC and healthy subjects.

Methods: Biomarker discovery was performed using Fourier transform ion cyclotron resonance mass spectrometry (FTICR-MS). Comprehensive metabolic profiles of CRC patients and controls from three independent populations from different continents (USA and Japan; total $n = 222$) were obtained and the best inter-study biomarkers determined. The structural characterization of these and related markers was performed using liquid chromatography (LC) MS/MS and nuclear magnetic resonance technologies. Clinical utility evaluations were performed using a targeted high-throughput triple-quadrupole multiple reaction monitoring (TQ-MRM) method for three biomarkers in two further independent populations from the USA and Japan (total $n = 220$).

Results: Comprehensive metabolomic analyses revealed significantly reduced levels of 28-36 carbon-containing hydroxylated polyunsaturated ultra long-chain fatty-acids in all three independent cohorts of CRC patient samples relative to controls. Structure elucidation studies on the C28 molecules revealed two families harbouring specifically two or three hydroxyl substitutions and varying degrees of unsaturation. The TQ-MRM method successfully validated the FTICR-MS results in two further independent studies. In total, biomarkers in five independent populations across two continental regions were evaluated (three populations by FTICR-MS and two by TQ-MRM). The resultant receiver-operator characteristic curve AUCs ranged from 0.85 to 0.98 (average = 0.91 ± 0.04).

Conclusions: A novel comprehensive metabolomics technology was used to identify a systemic metabolic dysregulation comprising previously unknown hydroxylated polyunsaturated ultra-long chain fatty acid metabolites in CRC patients. These metabolites are easily measurable in serum and a decrease in their concentration appears to be highly sensitive and specific for the presence of CRC, regardless of ethnic or geographic background. The measurement of these metabolites may represent an additional tool for the early detection and screening of CRC.

* Correspondence: s.ritchie@phenomenome.com
[1]Phenomenome Discoveries Inc, Saskatoon, SK, Canada

Background

Colorectal cancer (CRC) mortality remains one of the highest among all cancers, second to only lung cancer (Canadian Cancer Statistics, 2008). Despite the known benefits of early detection, screening programmes based on colonoscopy and fecal occult blood testing have been plagued with challenges such as public acceptance, cost, limited resources, accuracy and standardization. There is consensus in the field that the use of colonoscopy alone for CRC screening is not practical [1], and that a minimally-invasive serum-based test capable of accurately identifying subjects who are high risk for the development of CRC would result in a higher screening compliance than current approaches and better utilization of existing endoscopy resources [1-3]. Although there have been multiple reports of altered transcript levels [4-11], aberrantly methylated gene products [12-14] and proteomic patterns [15-18] associated with biological samples from CRC patients, few if any have advanced into clinically useful tests. This may be due to a number of reasons including technical hurdles in assay design, challenges obtaining reproducible results, costs and lengthy regulatory processes. Furthermore, most of the tests currently used or in development are based upon the detection of tumour-specific markers and have poor sensitivity for identifying subjects who are either very early stage, or are predisposed to risk but show no clinical presentation of disease.

Although causal genetic alterations for CRC have been well characterized, the number of cases due to adenomatous (APC) and hereditary nonpolyposs colorectal cancer are less than 5% of the total, with approximately 15% claimed to be attributable to inheritable family risk likely due to complex patterns of low penetrance mutations which have yet to be delineated [19]. The fact remains that approximately 80% of CRC cases are thought to arise sporadically, with diet and lifestyle as key risk factors [20,21]. In addition, an individual's microbiome is intricately linked to their gastrointestinal physiological status and may itself be involved as a risk factor [22]. Given that metabolism is heavily influenced by both diet and lifestyle and that the microbiome contributes its own metabolic processes, it is surprising that there has been little effort aimed identifying metabolic markers as risk indicators of CRC. This may, in part, have been due to the lack of platform technologies and informatics approaches capable of comprehensively characterizing metabolites in a similar way that DNA microarrays or surface-enhanced laser desorption ionization can characterize transcripts or proteins, respectively.

Recently, however, there have been rapid advances made in mass spectrometric-based systems which can identify large numbers of metabolic components within samples in a parallel manner [23-25]. Fourier transform ion cyclotron resonance mass spectrometry (FTICR-MS) is based upon the principle that charged particles exhibit cyclotron motion in a magnetic field, where the spin frequency is proportional the mass [26]. FTICR-MS is known for its high resolving power and capability of detecting ions with mass accuracy below 1 part per million (ppm). Liquid sample extracts can be directly infused using electrospray ionization (ESI) and atmospheric pressure chemical ionization (APCI) without chromatographic separation [23], where ions with differing mass to charge (m/z) ratios can be simultaneously resolved using a Fourier transformation. Using informatics approaches, spectral files from multiple samples can be accurately aligned and peak intensities across the samples compared [23]. High resolution also enables the prediction of elemental composition of all ions detected in a sample, providing a solid foundation for metabolite classification and identification, as well as the ability to construct *de novo* metabolic networks [23,27]. The combination of liquid extraction, flow injection, high resolution and informatics affords a unique opportunity to broadly characterize the biochemical composition of samples, with no *a priori* knowledge about the sample itself, to a degree which was not previously possible. This 'non-targeted' approach has the advantage of detecting novel compounds and is therefore ideally suited for biomarker-driven discovery applications. Using a MS-based discovery platform for metabolic biomarker identification also has the added advantage of straightforward translation into a quantitative method based upon triple-quadruple multiple-reaction-monitoring (TQ-MRM), similar to the clinical methods used to screen for inborn errors of metabolism [28].

Here we report on the application of this technology for characterizing the serum metabolomes of treatment-naive CRC patients and healthy asymptomatic subjects. A specific metabolic perturbation was discovered in the serum of CRC patients compared to controls in three independent and unrelated sets of samples (total n of 222). We further verify the perturbation using a tandem MS (MS/MS) approach in two additional independent case-control populations totalling 220 subjects. Implications of the findings for CRC screening are discussed.

Methods

Patient sample selection

Clinical samples used for the first discovery project were obtained from Genomics Collaborative, Inc (GCI, MA, USA), while samples for the second discovery project and one validation project were obtained from Seracare Lifesciences (MA, USA). These companies specialize in the collection and storage of serum and tissue samples

specifically for research purposes. Samples were collected, processed and stored in a consistent manner by teams of physicians as part of a global initiative using standardized protocols and operating procedures. Collection protocols for GCI and Seracare Lifesciences were approved by the Western Institutional Review Board and all samples were properly consented. The inclusion criterion for patient sample selection from the GCI and Seracare biobanks for both the discovery and validation cohorts was that the serum be taken prior to any form of treatment, including surgery, chemo or radiation therapies. All samples were accompanied by detailed pathology reports which were independently verified by certified pathologists at GCI and Seracare. The GCI discovery sample set included serum samples from 40 pretreatment CRC patients and matched 50 controls; the Seracare discovery set included samples from 26 pretreatment CRC and matched 25 controls, and the validation Seracare set included 70 pretreatment CRC and matched 70 controls. The discovery samples provided by Osaka Medical University (Osaka, Japan) included 46 pre-surgery CRC patients matched 35 controls which were prospectively collected according to the standard collection protocol of the institution and were properly consented. Study protocols were performed according to the ethical guidelines set by the committee of the three ministries of the Japanese Government. The samples for the Chiba, Japan, validation population, which included 40 pre-surgery CRC patients and 40 matched controls, were also prospectively consented and collected under an ethics reviewed protocol approved by the Institutional Review Board of Graduate School of Medicine, Chiba University. A summary of the populations including disease staging is shown in Table 1. All samples were processed and analysed in a randomized manner and the results unblinded following analysis.

Sample extraction

Serum samples were stored at -80°C until thawed for analysis and were only thawed once. All extractions were performed on ice. Serum samples were prepared for FTICR-MS analysis by first sequentially extracting equal volumes of serum with 1% ammonium hydroxide and ethyl acetate (EtOAc) three times. Samples were centrifuged between extractions at 4°C for 10 min at 3500 rpm and the organic layer removed and transferred to a new tube (extract A). A 1:5 ratio of EtOAc (extract A) to butanol (BuOH) was then evaporated under nitrogen to the original BuOH starting volume (extract B). All extracts were stored at -80°C until FTICR-MS analysis.

FTICR-MS analysis

For analysis under negative ESI conditions, sample extract B was diluted 10-fold in methanol:0.1% (v/v) ammonium hydroxide (50:50, v/v) prior to direct infusion. For APCI, extract A was directly injected without diluting. All analyses were performed on a Bruker Daltonics APEX III FTICR-MS equipped with a 7.0 T actively shielded superconducting magnet (Bruker Daltonics, MA, USA). Samples were directly injected using ESI and APCI at a flow rate of 600 μL per hour. Ion transfer/detection parameters were optimized using a standard mix of serine, tetra-alanine, reserpine, Hewlett-Packard tuning mix and the adrenocorticotrophic hormone fragment 4-10. In addition, the instrument conditions were tuned to optimize ion intensity and broadband accumulation over the mass range of 100-1000 atomic mass units (amu) according to the instrument manufacturer's recommendations. A mixture of the above mentioned standards was used to internally calibrate each sample spectrum for mass accuracy over the acquisition range of 100-1000 amu. FTICR data were

Table 1 Summary of case-control populations used in this study

	FTICR-MS discovery						MRM validation			
	Genomics Collaborative		Seracare 1		Osaka		Chiba		Seracare 2	
	CRC	Control	CRC	Control	CRC	Control	CRC	Control	CRC	Control
Total	40	50	26	25	46	35	40	40	70	70
Male *N*	19	24	17	16	27	-	19	24	44	41
Male age	59 (30-78)	56 (30-78)	62 (46-80)	51 (35-70)	63 (28-90)	-	68 (45-91)	48 (36-69)	67 (39-87)	63 (32-82)
Male BMI	20.9 ± 3.8	25.0 ± 0.9	24.3 ± 5.7	25.6 ± 4.6	NA	-	NA	NA	28.0 ± 4.8	26. ± 4.2
Female N	21	26	9	9	19	-	21	16	26	29
Female age	54 (40-82)	55 (40-79)	78 (59-86)	55 (26-95)	65 (31-77)	-	70 (51-84)	49 (39-59)	73 (35-90)	56 (26-86)
Female BMI	19.9 ± 4.6	24.8 ± 2.2	23 ± 3.2	29 ± 8.0	NA	-	NA	NA	25.5 ± 4.4	24.0 ± 4.5
Stage 0/I	8	-	5	-	10	-	9	-	13	-
Stage II	16	-	8	-	14	-	18	-	21	-
Stage III	15	-	8	-	12	-	11	-	25	-
Stage IV	1	-	2	-	8	-	2	-	7	-
Unknown	0	-	3	-	2	-	0	-	4	-

BMI = body mass index; CRC = colorectal cancer; FTICT-MS = Fourier transform ion cyclotron resonance mass spectroscopy; MRM = multiple reaction monitoring.

analysed using a linear least-squares regression line, mass axis values were calibrated such that each internal standard mass peak had a mass error of < 1 part ppm compared with its theoretical mass. Using XMASS software from Bruker Daltonics Inc (CA, USA), data file sizes of one megaword were acquired and zero-filled to two megawords. A SINm data transformation was performed prior to Fourier transform and magnitude calculations. The mass spectra from each analysis were integrated, creating a peak list that contained the accurate mass and absolute intensity of each peak. Compounds in the range of 100-1000 mz were analysed. In order to compare and summarize the data, all detected mass peaks were converted to their corresponding neutral masses, assuming hydrogen adduct formation. A self-generated two-dimensional (mass versus sample intensity) array was then created using *DISCOVA*-metrics™ software (Phenomenome Discoveries Inc, Saskatoon, Canada). The data from multiple files were integrated and this combined file was then processed in order to determine all of the unique masses. The average of each unique mass was determined, representing the *y*-axis. A column was created for each file that was originally selected to be analysed, representing the *x*-axis. The intensity for each mass found in each of the files selected was then filled into its representative *x,y* coordinate. Coordinates that did not contain an intensity value were left blank. Each of the spectra was then peak-picked in order to obtain the mass and intensity of all metabolites detected. The data from all modes were then merged to create one data file per sample. The data from all 90 discovery serum samples were then merged and aligned to create a two-dimensional metabolite array in which each sample is represented by a column, each unique metabolite is represented by a single row and each cell in the array corresponds to a metabolite intensity for a given sample. The array tables were then used for statistical analysis described in 'statistical analyses' (see Additional File 1).

Full-scan quadruple time-of-flight (Q-TOF) and high performance liquid chromatography (HPLC)-coupled MS/MS spectrometry

Ethyl acetate extracts from five CRC and five normal samples were evaporated under nitrogen gas and reconstituted in 70 μL of isopropanol:methanol:formic acid (10:90:0.1). Ten microlitres of the reconstituted sample was subjected to HPLC (HP 1100 with Hypersil ODS 5 μm, 125 × 4 mm column; Agilent Technologies, CA, USA) for full scan and 30 μL for MS/MS at a flow rate of 1 mL/min. Eluate from the HPLC was analysed using an ABI QSTAR® XL mass spectrometer fitted with an APCI source in negative mode. The scan type in full scan mode was TOF with an accumulation time of 1.0000 s, mass range between 50 and 1500 Da and duration time of 55 min. Source parameters were as follows: ion source gas (GS) 1 80; ion GS2 10; curtain gas (CUR) 30; nebulizer current (NC) -3.0; temperature 400°C; declustering potential (DP) -60; focusing potential (FP) -265; DP2 -15. In MS/MS mode, scan type was product ion, accumulation time was 1.0000 s, scan range between 50 and 650 Da and duration time 55 min. All source parameters are the same as above, with collision energy (CE) of -35 V and collision gas (CID, nitrogen) of 5 psi. For MS3 work, the excitation energy was set at 180 V.

Preliminary isolation of CRC biomarkers and NMR analysis

For the thin layer chromatographic methods, all chemicals and media were purchased from Sigma-Aldrich Canada Ltd (ON, Canada). All solvents were HPLC grade. Analytical thin layer chromatography (TLC) was carried out on pre-coated silica gel TLC aluminum sheets (EM Science, NJ, USA; Kieselgel 60 F_{254}, 5 × 2 cm × 0.2 mm). Compounds were visualized under ultraviolet light (254/366 nm) or placed in an iodine vapour tank and by dipping the plates in a 5% aqueous (w/v) phosphomolybdic acid solution containing 1% (w/v) ceric sulphate and 4% (v/v) H_2SO_4, followed by heating. NMR spectra were recorded on Bruker Avance spectrometers; for ^1H (500 MHz), δ values were referenced to $CDCl_3$ ($CHCl_3$ at 7.24 ppm) and for ^{13}C NMR (125.8 MHz) referenced to $CDCl_3$ (77.23 ppm).

Ethyl acetate extracts of commercial serum (180 mL serum, 500 mg extract) was subjected to reverse phase flash column chromatography (FCC) with a step gradient elution; acetonitrile - water 25:75 to 100% acetonitrile. The fractions collected were analysed by LC/MS and MS/MS. The fractions containing the CRC biomarkers were pooled (12.5 mg). This procedure was repeated several times to obtain about 60 mg of CRC biomarker rich fraction. This combined sample was then subjected to FCC with a step gradient elution; hexane-chloroform-methanol and the fractions collected subjected to LC/MS and MS/MS analysis. The biomarker rich fraction labelled sample A (5.4 mg, about 65%) was analysed by NMR. Sample A (3 mg) was then treated with excess ethereal diazomethane and kept overnight at room temperature. After the removal of solvent, the sample was analyzed by NMR.

TQ-MRM methodology

Serum samples were extracted as described for non-targeted FTICR-MS analysis, with the addition of 10 ug/mL [$^{13}C_1$]cholic acid to the serum prior to extraction (resulting in a final ethyl acetate concentration of [$^{13}C_1$] cholic acid of 36 nM. The ethyl acetate organic fraction was used for the analysis of each sample. A series of

[$^{13}C_1$]cholic acid dilutions in ethyl acetate from Randox serum extracts was used to generate a standard curve ranging between 0.00022 μg/mL and 0.222 μg/mL. 100 μL of sample were injected by flow-injection analysis into the 4000QTRAP™ equipped with a TurboV™ source with an APCI probe. The carrier solvent was 90% methanol:10% ethyl acetate, with a flow rate of 360 μL/min into the APCI source. The source gas parameters were as follows: CUR: 10.0, CAD: 6, NC: -3.0, TEM: 400, GS1: 15, interface heater on. 'Compound' settings were as follows: entrance potential (EP): -10, and collision cell exit potential (CXP): -20.0. The method is based on the MRM of one parent ion transition for each of the C28 molecules (445.3-383.4 Da, 447.4-385.4 Da, and 449.4-405.4 Da) and a single transition for the internal standard (408.3-343.4 Da). Each of the transitions was monitored for 250 ms for a total cycle time of 2.3 s. The total acquisition time per sample was approximately 1 min. All accepted analyses showed R^2 correlation coefficients for the linear regression equation of >0.98. [$^{13}C_1$]cholic acid equivalents for each of the three C28 molecules were calculated by determining the percent recovery of [$^{13}C_1$]cholic acid in each sample by dividing the extrapolated concentration by 0.0148 ug/ml (36 nM, the theoretical amount present in the ethyl acetate extract of each sample). Metabolite concentrations represented as [$^{13}C_1$]cholic acid equivalents were then extrapolated, normalized by dividing by the percent recovery and multiplied by appropriate extraction dilution factors to yield a final serum concentration.

Statistical analysis

FTICR-MS accurate mass array alignments were performed using *DISCOVA*metrics™ version 3.0 (Phenomenome Discoveries Inc, Saskatoon, Canada). Statistical analysis and graphs of FTICR-MS data was carried out using Microsoft Office Excel 2007 and distribution analysis of TQ-MRM data and was analysed using JMP version 8.0.1. Meta Analysis (Fisher's inverse chi-square method) was carried out using SAS 9.2 and R 2.9.0. Two-tailed unpaired Student's *t*-tests were used for determination of significance between CRC and controls. *P*-values of less than 0.05 were considered significant. Receiver operating curve (ROC) curves were generated using the continuous data mode of JROCFIT http://www.jrocfit.org.

Results

FTICR metabolomic profiling

The experimental workflow for the studies described in this paper is summarized in Figure 1. Non-targeted metabolomic profiles of sera from three independent populations of treatment-naive CRC patients and geographically and ethnically matched healthy controls (summarized in Table 1) were generated over a 24-month period (that is, each study was separated by approximately 12 months). The first study comprised 40 CRC patients and 50 control subjects acquired from Genomics Collaborative, Inc (GCI); the second study comprised 26 CRC subjects and 25 controls acquired from Seracare Lifesciences Inc; and the third study included 46 CRC and 35 controls prospectively collected in Osaka, Japan. In all cases, serum metabolites were captured through a liquid extraction process (see Methods), followed by direct infusion of the extracts using negative electrospray ionization (nESI) and negative atmospheric pressure chemical ionization (nAPCI) on an FTICR mass spectrometer. The resulting spectral data of all the subjects for each study was aligned within 1 ppm mass accuracy, background peaks were subtracted, and a two-dimensional array table comprising the intensities each of the sample-specific spectral peaks was created using custom informatics software (see Methods). Metabolic differences between CRC patient and control profiles for the three independent studies were visualized by plotting the control mean-normalized log ratio peak intensities across the detected mass range as shown in Figures 2A to 2C. In each independent study, a region of spectra between approximately 440 and 600 Da showed peaks consistently reduced in intensity in CRC patients relative to controls (green, yellow, orange and red points in Figure 2). On average, this cluster of masses showed between 50% and 75% reduction in CRC patient serum compared to the respective controls, with p-values of 1×10^{-5} or lower in each study.

The overlap between each of the discovery studies was further investigated by ranking the top 50 masses based upon *P*-value from each study and comparing them with masses showing a significant difference ($P < 0.05$ between CRC and controls) in the other studies as shown in Table 2. For example, 46 of the top 50 metabolites (92%) with the lowest p-values in the GCI discovery set were also significant ($P < 0.05$) in the Seracare 1 dataset, while 31 out of the 50 GCI masses were significant ($P < 0.05$) in the Osaka dataset. Likewise, the top 50 metabolites in the Osaka study showed 88% and 94% redundancy with metabolites showing $P < 0.05$ in the GCI and Seracare 1 studies, respectively. These results indicated a very high degree of commonality among significantly differentiated masses across the three studies, and in fact, 63% of the top 50 masses in each study were also present within the top 50 of at least one of the other two studies (see Additional File 2). Of the top 50 rank-ordered masses, only those identified in more than one study were found to exist within the 440 to 600 Da mass range highlighted above and there was not a single peak detected outside this region which was significantly different between CRCs and controls in any two of the studies. Filtering for metabolic differences detected exclusively in all three studies (as well as removal of C13 isotopic peaks and redundant masses

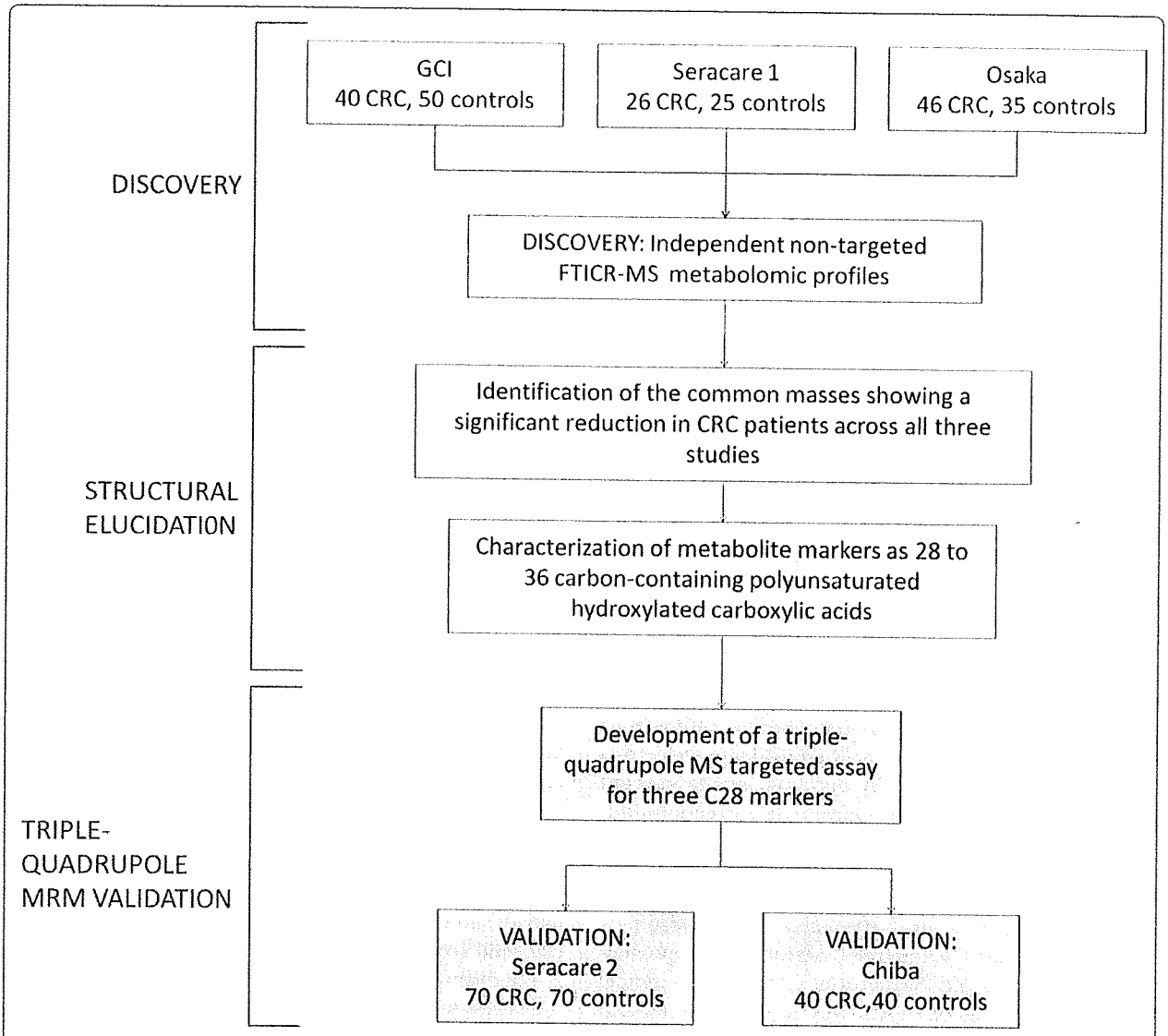

Figure 1 Study design. The study comprised three phases: Fourier transform ion cyclotron resonance mass spectrometry metabolomic discovery in three independent sample sets, structural investigation and determination of metabolic biomarkers as hydroxylated polyunsaturated ultra long-chain fatty acids and validation using a triple-quadrupole multiple reaction monitoring targeted assay.

detected in both ESI and APCI), resulted in 13 masses representing individual ^{12}C metabolites as shown in Table 3. These represented the most statistically significant and robust discriminators among the three studies. Subsequent molecular formula assignments, as discussed further below, as well as related expression profiles, suggested that the metabolites belonged to a related chemical family.

The relative intensities of the two lowest molecular weight molecules with nominal masses of 446 and 448 are shown in Figure 3A. We observed little to no correlation between the reduction of the metabolites and disease stage (Figures 3A and 3B), and ROC curve analysis resulted in an average area under-the-curve (AUC) of 0.91 ± 0.03 (Figure 3C; individual AUCs shown) across all three studies for all stages combined.

Computational assignments of reasonable molecular formulas were then carried out for the 13 masses identified above, as well as the top 50 for each discovery set shown in Additional File 2. The assignments were based on a series of mathematical and chemometric rules as described previously [23], which are reliant on high mass accuracy for precise prediction. The algorithm computes the number of carbons, hydrogens, oxygens and other elements, based on their exact mass, which can be assigned to a detected accurate mass within defined constraints. Logical putative molecular formulas were

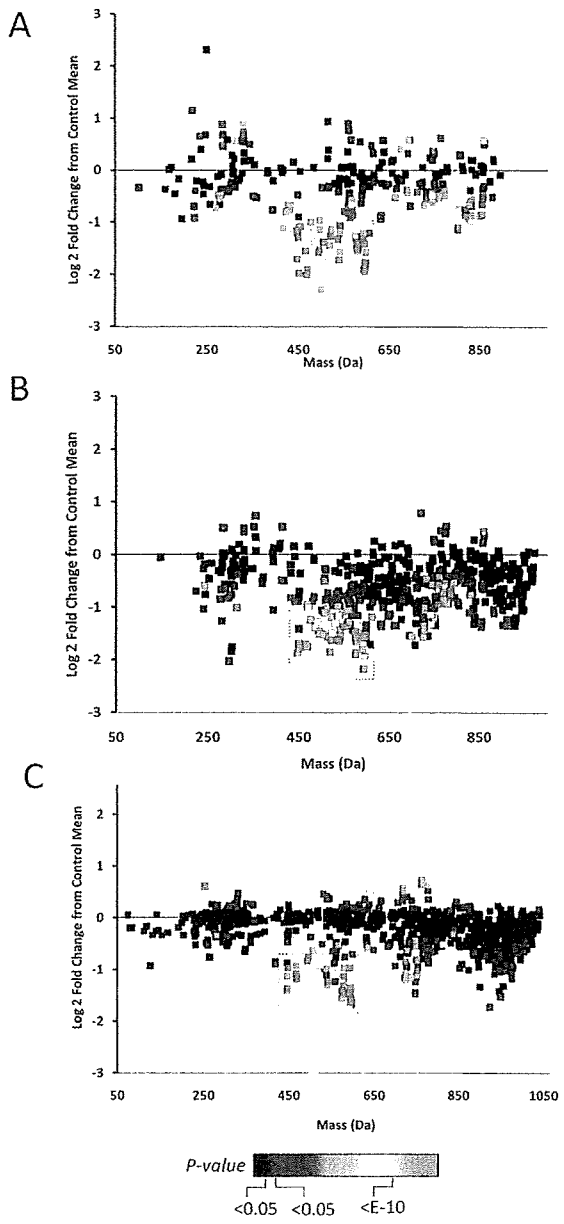

Figure 2 Scatter plots of average sample peak intensity fold change between colorectal cancer (CRC) and normal patient sera in three independent studies. Sample-specific peaks for all subjects were log2 normalized to the mean of the control population, and plotted according to mass (Da). Points are coloured according to significance based on an unpaired Students't-test (see legend). (A) Genomics Collaborative Inc discovery population, (B) Seracare 1 discovery population, (C) Osaka discovery population. The region boxed in grey represents the cluster of masses between 440 and 600 Da consistently reduced in the CRC patient population compared to controls in all three cohorts.

computed for masses in Table 3 (and Additional File 2), resulting in elemental compositions containing either 28, 30, 32 or 36 carbons and four to six oxygen. We used this information in the subsequent section to select appropriate molecules for structural comparison studies. Collectively, the results indicated a consistent 50% to 75% reduction of organically soluble oxygenated metabolites ranging between 28 and 36 carbons in length, in the serum of CRC patients compared to controls.

Structural elucidation

Selected ethyl acetate extracts of serum from the GCI cohort used in the FTICR-MS work described above were re-analysed using HPLC coupled to a quadrupole time-of-flight (Q-TOF) MS in full-scan APCI negative ion mode. Consistent with the FTICR-MS results, a cluster of peaks between approximately 440 and 600 Da at a retention time of between 16 and 18 min following reverse-phase HPLC was detected in asymptomatic control sera, but was absent from CRC patient serum (Figure 4). Molecular ions from all six C28 biomarkers (m/z 446, m/z 448, m/z 450, m/z 464, m/z 466 and m/z 468) as well as many of the remaining C32 and C36 markers were easily detectable within normal serum. Extracted masses up to 400 Da within the 16-18 min retention time showed similar peak intensities in both populations (Figure 4, region to the right of the box), as did extracted mass spectra at other retention times (not shown), reinforcing the specificity of this depleted metabolic region for CRC patient serum.

Tandem mass spectrometric fragmentation fingerprints were next generated for the six C28 biomarkers (Table 4, see Additional Files 345678) and for the higher C32 and C36 biomarkers (see Additional File 9). The MS/MS and MS3 fragmentation data of the six C28 biomarkers were dominated by peaks resulting from losses of H_2O (m/z 427, 429, 431, 445, 447 and 449), losses of two molecules of H_2O (m/z 409, 411, 413, 427, 429, 431), losses of CO_2 (m/z 401, 403, 405, 419, 421, 423) and losses of CO_2 and H_2O (m/z 383, 385, 387, 401, 403, 405), indicating the presence of carboxylic acid functionality and two or more hydroxyl groups. The molecular formulae, organic properties of the molecules and the tandem MS data suggested that the metabolites were derivatives or analogues of one or more possible classes of molecules including fat soluble vitamins such as retinol and retinoic acid (vitamin A), calciferols (vitamin D), tocopherols (vitamin E), phylloquinones (vitamin K), steroids or bile acids, or long chain polyunsaturated hydroxy fatty acids. Tandem mass spectrometric fragmentation fingerprints of standards for each of these metabolic classes were therefore generated including 5S,6S-(7E,9E,11Z,14Z)-dihydroxyeicosatetraenoic acid (**1**), 15S-Hydroxy-(5Z,8Z,11Z,13E)-